Development of 3D-printed micro-lenses at the edge of waveguides of flow cytometry and optical coherence tomography photonic integrated circuits

A. M. Grammatikaki[a,b], L. Gounaridis[a,b], D. Gounaridis[a,b], K. Obara[c], A. Everhardt[d], A. Raptakis[a,b], Ton G. van Leeuwen[e], E. van der Pol[e], H. Avramopoulos[a,b], C. Kouloumentas[a,b]
[a]Institute of Communication and Computer System, 42 Patission, Athens, Greece, [b]National Technical University of Athens, 9 Iroon Polytechneiou, Zografou, Greece, [c]PHIX Photonics Assembly,
De Veldmaat 17, 7522 NM Enschede, The Neatherlands, [d]LioniX International BV, Hengelosestraat 500, Enschede, 7521 AN, The Neatherlands, [e]Amsterdam UMC, Meibergdreef 9 1105 AZ Amsterdam, The Neatherlands

ABSTRACT

Flow cytometry (FCM) contributes significantly to healthcare by enabling the rapid and accurate analysis of cell populations, which enhances our ability to diagnose, monitor, and assess treatment for conditions such as cancer and stroke. A multi-sensing biophotonic platform has been designed, integrating innovative FCM and Optical Coherence Tomography (OCT) photonic integrated circuits (PICs) and focusing on the detection of extracellular vesicles (EVs) down to 140 nm. The OCT module is utilized to ensure the validity of FCM measurements. The platform's micro-optic elements, designed for light manipulation within the sensing PICs, serve as interfaces between the photonic and fluidic components. Focusing lenses illuminate and collect light at specific flow channel points for FCM measurements at wavelengths of 520 and 638 nm, while the OCT module uses focusing micro-lenses for illumination and collection at 790 nm. This work presents the design, fabrication, and testing of the micro-lenses, achieving optical losses as low as 0.3 dB, equivalent to a coupling efficiency of up to 93%.

Keywords: Photonic integrated circuits, 3D-printed micro-lenses, Silicon nitride platform, flow cytometry, extracellular vesicles

1. INTRODUCTION

Modern medicine strives to address major health threats, such as cancer and cardiovascular diseases [1][2][3]. Crucial insights lie in circulating cells, vesicles, and molecules within blood, necessitating tools that connect macroscopic and microscopic imaging [4]. In this context, EVs play a pivotal role in waste removal and intercellular communication [5][6]. Using EVs as biomarkers provides valuable information about their cellular origins, aiding in disease detection and progression tracking. However, detecting EVs in blood samples is groundbreaking but challenging due to their small size (80-1000 nm) [7].

The current study is part of the PHOREVER project, which aims to develop a compact, low-cost multi-sensing biophotonic platform as a point-of-care device. This platform is designed to detect EVs as small as 140 nm, identify disease-specific proteins on EV membranes, quantify EV concentrations in blood samples, and potentially define specific EVs as new biomarkers. Its goal is to revolutionize disease diagnosis, monitoring, and treatment assessment for conditions such as cancer and stroke [8].

An innovative FCM module based on the TriPleX platform will measure EV concentrations through angular scattering and fluorescence sensing [9][10]. An OCT module on the same platform will estimate particle numbers to validate FCM

Integrated Optics: Devices, Materials, and Technologies XXIX, edited by Sonia M. García-Blanco, Pavel Cheben, Proc. of SPIE Vol. 13369, 133690V · © 2025 SPIE
0277-786X · doi: 10.1117/12.3042890

measurements. Both PICs will be integrated into the platform's non-disposable core, with a disposable microfluidic unit for automated blood sample analysis. AI and data analysis tools will use EVs as biomarkers for pancreatic and stroke diseases.

The study focuses on the platform's micro-optic elements, specifically the design, fabrication, and evaluation of 3D-printed lenses for light manipulation within the sensing PICs [11]. These lenses serve as interfaces between the photonic and fluidic components. Focusing lenses were developed to illuminate and collect light at specific flow channel points for FCM and fluorescence measurements at 520 nm and 638 nm, while the OCT module uses micro-lenses for illumination and collection at 790 nm. The simulation and characterization results for the lenses' coupling efficiency showed good agreement, with total losses measured below 0.7 dB.

2. SIMULATION STUDY

2.1 Simulation platform

Zemax is a versatile and powerful software tool widely used in optical design, particularly for micro-lens design [12][11]. It provides a user-friendly environment for defining the geometry, materials, and optical properties of micro-lenses and includes advanced ray tracing capabilities to simulate light behavior and assess performance. With specialized lens design tools, users can specify parameters such as shape, curvature, thickness, and refractive index, while optimization algorithms enable iterative improvements to achieve specific goals like minimizing aberrations or optimizing light transmission. Zemax also offers robust performance analysis tools, including spot diagrams, wavefront analysis, and modulation transfer function (MTF) calculations, to evaluate factors like image quality and resolution. Additionally, the software supports tolerancing to assess manufacturing variations, integrates seamlessly with other tools and CAD packages, and provides comprehensive documentation and reporting features. These capabilities make Zemax an essential tool for designing, analyzing, optimizing, and documenting micro-lenses within optical systems.

2.2 Component design

Before integrating the lenses onto the PICs, an intermediate step was conducted to evaluate the designs and fabrication processes. During this phase, the lenses were 3D-printed at the edge of fiber array units (FAUs) to facilitate testing and analysis [13]. Designs were developed for four distinct focusing lenses, optimized for specific wavelengths: 520 nm, 638 nm, and two variations for 790 nm [Figure 1]. This approach ensured the optimization of lens performance prior to their integration into the PICs. The distance between the transmitting and receiving lenses was set to 2.5 mm, as required by the PICs. Specifically, this distance matches the diameter of the through-hole in both modules of the PICs, which is designed for the passage of the biofluids.

During the simulation procedure there were two designs at 790 nm performing optimally in terms of focusing and coupling efficiency. These two designs (namely type-1 and -2), have similar geometrical parameters. We decided to fabricate both and obtain an experimental perspective and familiarity with the structures. Together with the best-performing structures at 520 nm and 638 nm, they were sent for fabrication, where they were 3D-printed at the edges of the FAUs.

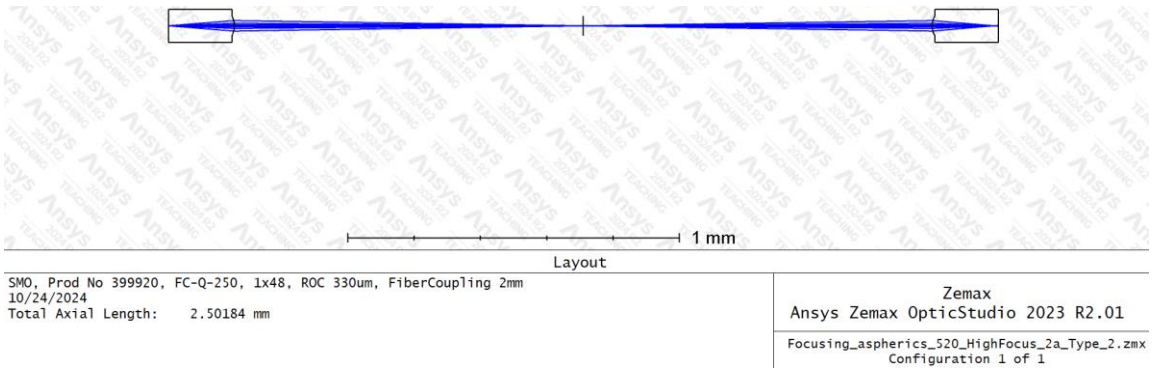

Figure 1 Example of simulation setup in ZEMAX for lenses' design

3. FABRICATION PROCESS

3.1 Hardware and materials

The micro-lenses were 3D printed using two-photon polymerization process, which relies on the simultaneous absorption of two photons in a photosensitive material (photoresist). This process leads to local polymerization of the resist by locally activating the photo-initiator with light at a wavelength of 785 nm. The Nanoscribe Quantum X Align system was used for printing, utilizing a standard IP-S organic resin, which exhibits ~90% transmittance in the spectral range of 650 nm to 1550 nm.

Once printed, the lenses undergo quality control through a comparative analysis of the theoretical high-resolution solid 3D model and the experimentally measured geometry, using the MarSurf CM Explorer system. Optical and confocal microscopy methods are employed for this quality control. Reliability trials were conducted to determine how optical, thermal, and mechanical phenomena affect the performance of the 3D printed lenses. More information on 3D printed lens reliability studies can be found in Table 1. An example of a lens array 3D printed on the facet of a FAU is shown in Figure 2.

Table 1 3D printed lens reliability testing

Test type	Methodology	Purpose (aspect to be determined)
Optical	Transmission measurements	Impact of coupled laser light on transmission losses
Thermal	Annealing	Impact of temperature on transmission losses
Mechanical	Shear testing	Lens adherence to the substrate

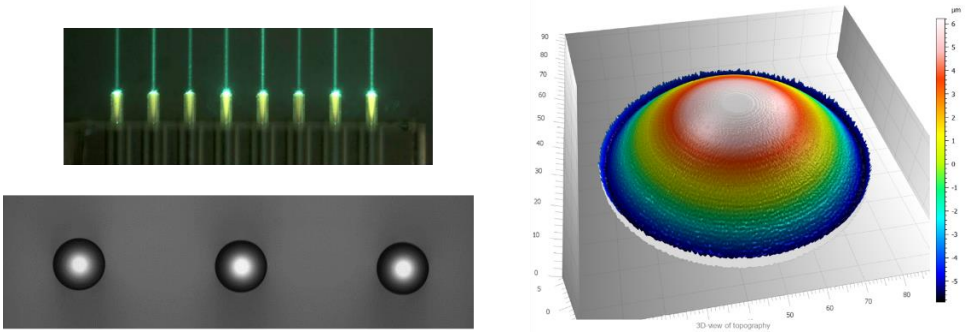

Figure 2 Example of 3D printed lenses from a related experiment: top-left: photography of a lens array printed on fibre array's facet, bottom-left: confocal microscope image presenting top view of three lenses in an array, right: confocal microscope surface analysis for an individual lens

3.2 Fabrication steps

As previously described, the lens 3D printing process utilized a two-photon lithography technique, an additive manufacturing method for developing volumetric optical structures. This process involves local curing of an organic resin with radiation emitted by a femtosecond laser beam operating at a wavelength of 785 nm. Energy from the laser promotes polymerization of the organic resin at the focal point of the beam, which is steered point-by-point across the XY-axis plane within the field of view of a microscope objective using a set of mirrors. Once all volumetric pixels (voxels) for a given Z-axis level (height) are completed, the focus shifts in altitude to construct the next level of the structure. After the lens is fully formed, the residual resin is removed with an organic solvent.

An example of this process is illustrated in Figure 3, showing a schematic, step-by-step guide for printing on the top surface of a PIC over a grating coupler. In order to 3D print a micro-lens on a side facet (or on surface) of a PIC, specific alignment fiducials are required in form of a checkerboard in waveguide material layer of TriPleX platform.

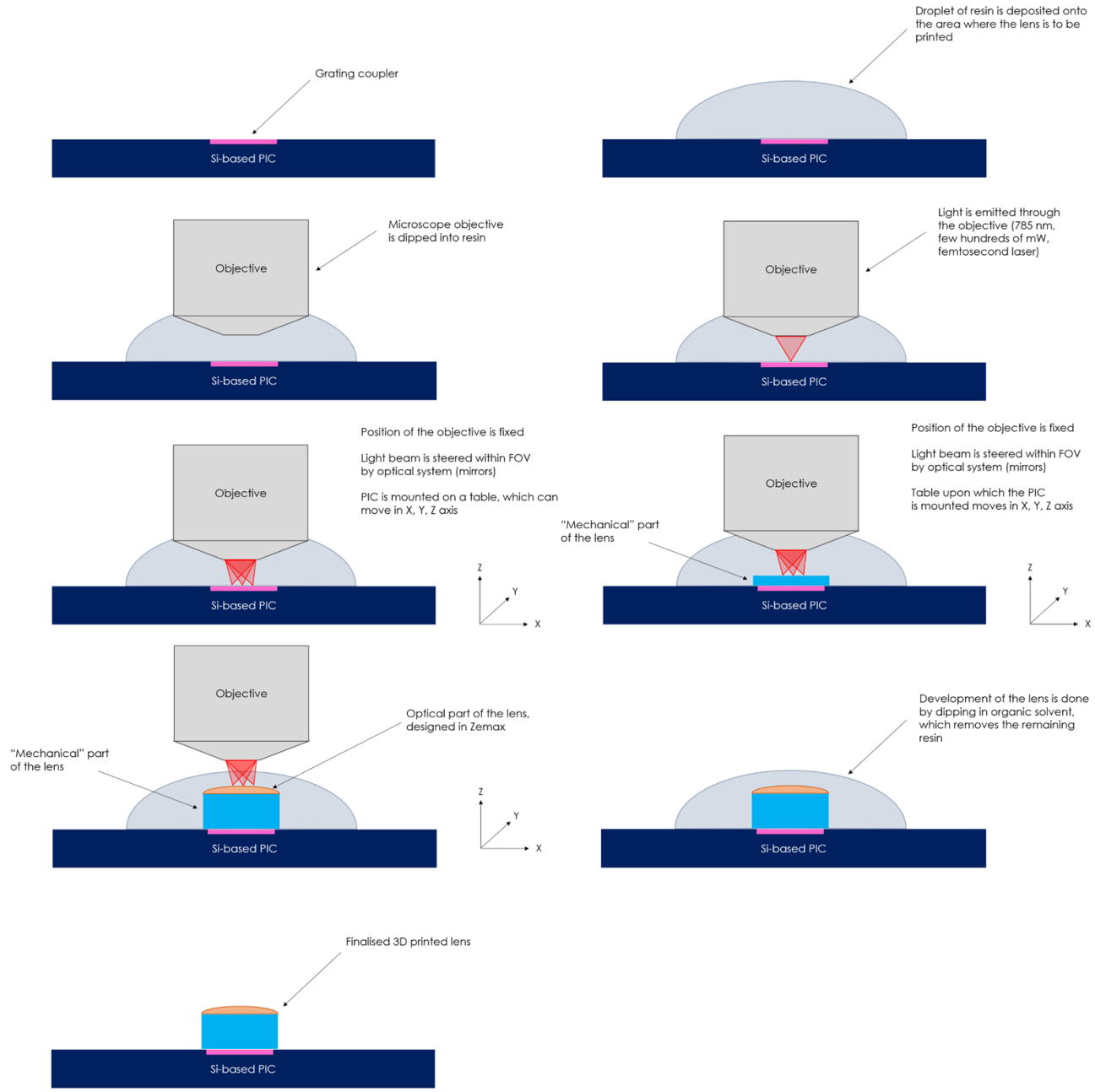

Figure 3 Lens 3D printing process principle

To summarize the procedure, for the four different designs of micro-lenses, once their custom designs were finalized, a 3D model was generated by the fabricator, comprising both optical and mechanical components. The next step involved 3D printing the lenses on the facet of two FAUs. Finally, the fabricated lenses underwent thorough quality and reliability testing to ensure they met the required specifications (Figure 4).

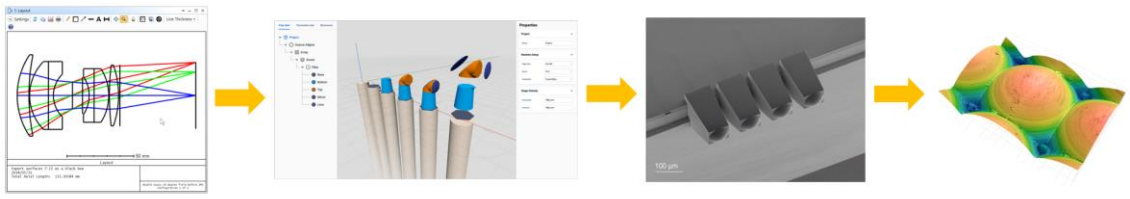

Figure 4 Flowchart of 3D lens fabrication

4. MEASUREMENT PROCEDURE

The lenses were characterized by measuring their coupling efficiency to evaluate their optical performance. For each wavelength, sixteen identical micro-lenses were 3D printed on the facets of two FAUs, with eight lenses on each FAU. Three lenses from one FAU were used as emitters, while all eight lenses on the second FAU were used as receivers. This configuration resulted in 3x8 unique lens pairs being tested, ensuring the reliability of the measurements.

4.1 Experimental setup

The system set for the measurement of the coupling efficiency of the lenses consisted of several key components [Figure 5]. These include three lasers operating at specific wavelengths (520 nm, 638 nm and 850 nm), patch cords for ensuring the appropriate fiber connections, an attenuator to control the laser power, and two optical power meters. The focusing lenses designed for 520 nm and 638 nm were tested at their respective wavelengths, while the lenses designed for 790 nm were tested using an 850 nm laser.

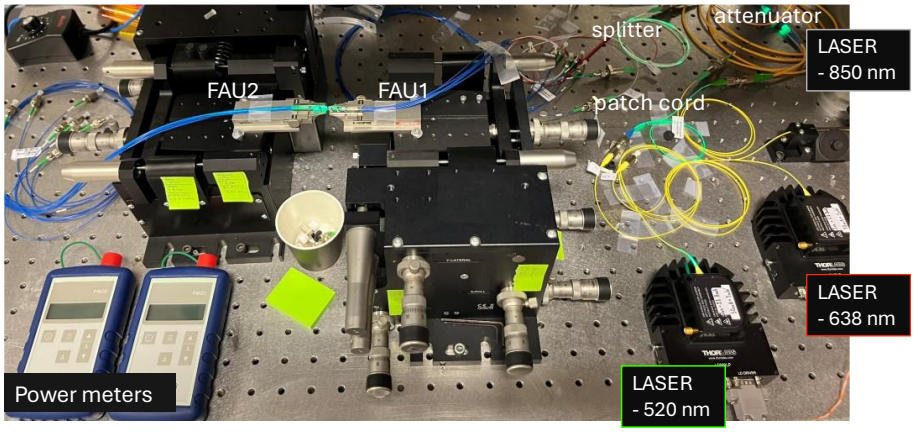

Figure 5 Experimental setup for the lenses' evaluation

First the laser source at the designated wavelength was connected to an attenuator through a patch cord. The attenuator was used to ensure that the optical power reaching the lenses was at the desired level (0 dB), while the laser operated within its optimal range to provide reliable performance. The lenses printed on the first FAU were considered the emitting lenses in the setup, whereas those printed on the second FAU were responsible for receiving the light. Alignment was performed using two 6-axis flexure stages, though the exact distance between lenses could not be measured. Finally, power meters were utilized to measure the optical power at the outputs of the FAUs, as well as at various intermediate stages throughout the setup.

4.2 Testing procedure

After assembling the experimental setup, we set the laser temperature to 25°C and powered it with a current that ensured a stable and reliable optical output power. The attenuator was then manipulated so that the optical output power of the first

FAU lens would be 0 dBm. This was measured free space with an optical power meter. The alignment process involved manipulating the 6-axis flexure stages to achieve the highest possible optical output power from the second FAU. Once the emitting lens under consideration was aligned with all receiving lenses, the losses for each pair were measured using the following formula:

$$Pout_{FAU_1} - Pout_{FAU_2} - FAU_2\ losses$$

, where the losses introduced by the second FAU, related to its connection to the power meters, were considered to be approximately 0.2 dB, as specified by the manufacturer.
After these measurements, the output power from the emitting lens was re-measured to ensure consistency. This procedure was repeated for three different lenses of the first FAU.

5. MEASUREMENT RESULTS

The coupling efficiency of 3x8 unique lens pairs was evaluated to study the optical performance of the lenses. The measurements were expressed in terms of optical losses (dB) and then translated into their corresponding efficiency values.

The lenses tested at 520 nm and 638 nm showed efficient coupling with minimal optical losses. For the 520 nm lenses, the lowest losses observed were 0.3 dB, while the 638 nm lenses had a minimum loss of 0.4 dB. The results across the three measurement sets for the emission lenses were consistent, indicating a uniform fabrication process. However, in each set, the outermost lenses (Lenses 1 and 2) exhibited slightly reduced coupling efficiency, particularly in the 520 nm lenses, though this effect was also noted to a lesser degree in the 790 nm lenses. While the exact cause—potentially alignment limitations, and less likely, fabrication imperfections or minor damage to the lenses—remains uncertain, the consistency of this pattern indicates that these deviations are not significant enough to impact overall lens performance. In summary, an accuracy of up to 93% was achieved for the 520 nm lenses and 91% for the 638 nm lenses.

Table 2 Coupling losses (in dB) for micro-lenses at 520 nm

Output lenses	**Input lens 1**	**Input lens 2**	**Input lens 3**
1	1.1	1.3	1.2
2	0.7	0.5	0.6
3	0.5	0.4	0.5
4	0.4	0.3	0.4
5	0.4	0.3	0.3
6	0.3	0.3	0.3
7	0.4	0.3	0.4
8	0.4	0.4	0.4
Mean/ Std.	~0.5 dB, ~0.2	~0.5 dB, ~0.3	~0.5 dB, ~0.3

Table 3 Coupling losses (in dB) for micro-lenses at 638 nm

Output lenses	**Input lens 1**	**Input lens 2**	**Input lens 3**
1	0.6	0.7	0.6
2	0.5	0.6	0.5
3	0.4	0.4	0.4
4	0.4	0.5	0.5
5	0.4	0.4	0.5
6	0.4	0.4	0.4
7	0.4	0.4	0.4
8	0.4	0.5	0.5
Mean/ Std.	~0.4 dB, <0.1	~0.5 dB, ~0.1	~0.5 dB, <0.1

The lenses optimized for 790 nm and tested at 850 nm demonstrated efficient coupling, though slightly less effective compared to the lenses designed and tested at their respective wavelengths. This is likely due to the difference between the design and testing wavelengths. Both types of 790 nm lenses exhibited a minimum loss of 0.7 dB with relative uniformity across the various pair measurements, indicating consistency and reliability in the fabrication and evaluation processes. As with the previous lenses, the outermost lenses showed the lowest efficiency. The measurements indicated an efficiency of up to 85%, suggesting that the coupling efficiency would likely improve when the lenses are tested and used at their intended wavelength.

Table 4 Coupling losses (in dB) for micro-lenses at 790 nm - Type 1

Output lenses	**Input lens 1**	**Input lens 2**	**Input lens 3**
1	1.1	1.1	1.0
2	1.2	1.1	1.0
3	0.9	0.8	0.9
4	0.8	0.9	0.9
5	0.7	0.9	0.8
6	0.8	0.8	0.8
7	0.9	1.0	0.9
8	0.8	0.8	0.8
Mean/ Std.	~0.9 dB, ~0.16	~0.9 dB, ~0.12	~0.9 dB, <0.1

Table 5 Coupling losses (in dB) for micro-lenses at 790 nm - Type 2

Output lenses	**Input lens 1**	**Input lens 2**	**Input lens 3**
1	0.7	0.9	0.7
2	0.8	0.9	0.7
3	0.8	0.9	0.7
4	0.8	1.0	0.7
5	0.8	0.9	0.7
6	0.8	0.9	0.7
7	0.9	1.0	0.8
8	0.9	1.0	0.8
Mean/ Std.	~0.8 dB, < 0.1	~0.9 dB, < 0.1	~0.7 dB, < 0.1

6. CONCLUSIONS

This study successfully demonstrated the design, fabrication, and evaluation of 3D-printed micro-lenses for photonic integrated circuits. The micro-lenses were specifically designed for 520 nm and 638 nm wavelengths for the FCM module and 790 nm for the OCT module. While the designs presented here are tailored for FCM and OCT applications, this study also provides valuable general insights into their development and performance. Characterization results showed coupling losses as low as 0.3 dB for the 520 nm lenses, 0.4 dB for the 638 nm lenses, and 0.7 dB for the 790 nm lenses when tested at 850 nm. These results correspond to coupling efficiencies of 93%, 91%, and 85%, respectively. Lenses tested at non-optimized wavelengths are expected to achieve even higher efficiencies when operated at their intended design wavelengths. The consistent performance across the measured sets further supports the reliability of the design, fabrication, and evaluation processes. This study highlights the potential of 3D-printed micro-lenses to achieve high coupling efficiencies, offering a reliable and scalable solution for enhancing optical performance in photonic integrated circuits designed for advanced sensing technologies.

ACKNOWLEDGEMENTS

This work is a part of the PHOREVER project. This project has received funding from the European Union's Horizon 2022 research and innovation program under grant agreement No 101093171. Content reflects only the authors' view, and the Research Executive Agency (REA) / European Commission is not responsible for any use that may be made of the information it contains.

REFERENCES

[1] E. J. Benjamin et al., "Heart Disease and Stroke Statistics-2019 Update: A Report From the American Heart Association," 139(10), Circulation, e56–e528 (2019); https://doi.org/10.1161/CIR.0000000000000659.
[2] H. A. Wafa et al., "Burden of Stroke in Europe: Thirty-Year Projections of Incidence, Prevalence, Deaths, and Disability-Adjusted Life Years," 51(8), Stroke, 2418–2427 (2020); https://doi.org/10.1161/STROKEAHA.120.029606.
[3] A. D. Singhi et al., "Early Detection of Pancreatic Cancer: Opportunities and Challenges," 156(7), Gastroenterology, 2024–2040 (2019); https://doi.org/10.1053/j.gastro.2019.01.259.
[4] E. van der Pol et al., "Optical and Non-Optical Methods for Detection and Characterization of Microparticles and Exosomes," 8(12), Journal of Thrombosis and Haemostasis, 2596–2607 (2010); https://doi.org/10.1111/j.1538-7836.2010.04074.x.
[5] L. M. Doyle et al., "Overview of Extracellular Vesicles, Their Origin, Composition, Purpose, and Methods for Exosome Isolation and Analysis," 8(7), Cells, 727 (2019); https://doi.org/10.3390/cells8070727.
[6] E. van der Pol et al., "Classification, Functions, and Clinical Relevance of Extracellular Vesicles," 64(3), Pharmacological Reviews, 676–705 (2012); https://doi.org/10.1124/pr.112.005983.
[7] M. Kuiper et al., "Reliable Measurements of Extracellular Vesicles by Clinical Flow Cytometry," 85(2), American Journal of Reproductive Immunology, e13350 (2021); https://doi.org/10.1111/aji.13350.
[8] K. T. Stenz et al., "Extracellular Vesicles in Acute Stroke Diagnostics," 8(8), Biomedicines, 248 (2020); https://doi.org/10.3390/biomedicines8080248.
[9] K. Wörhoff et al., "TriPleX: A Versatile Dielectric Photonic Platform," 4(2), Advanced Optical Technologies, 189–207 (2015); https://doi.org/10.1515/aot-2015-0016.
[10] J. Botha et al., "Conventional, High-Resolution and Imaging Flow Cytometry: Benchmarking Performance in Characterisation of Extracellular Vesicles," 9(2), Biomedicines, 124 (2021); https://doi.org/10.3390/biomedicines9020124.
[11] S. Yu et al., "Two-photon lithography for integrated photonic packaging," 4, Light: Advanced Manufacturing, 39 (2023); https://doi.org/10.37188/lam.2023.032 ANSYS,
[12] "ANSYS Zemax OpticStudio," accessed on Jan 2025, https://www.ansys.com/products/optics/ansys-zemax-opticstudio.
[13] A. Çalıkoğlu et al., "3D Nano-Printed Bistable Microlens Actuator for Reconfigurable Micro-Optical Systems," 34, Advanced Functional Materials (2024); https://doi.org/10.1002/adfm.202408867.